

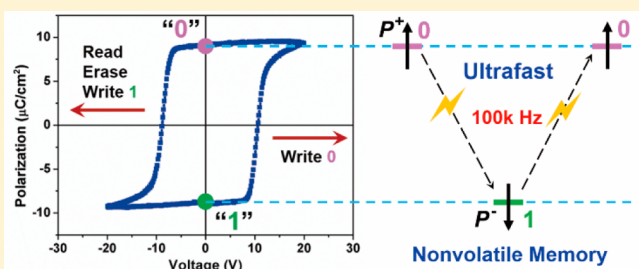
A Multiaxial Molecular Ferroelectric with Highest Curie Temperature and Fastest Polarization Switching

Yuan-Yuan Tang, Peng-Fei Li, Wan-Ying Zhang, Heng-Yun Ye, Yu-Meng You,* and Ren-Gen Xiong*^{†,ID}

Ordered Matter Science Research Center, and Jiangsu Key Laboratory for Science and Applications of Molecular Ferroelectrics, Southeast University, Nanjing 211189, P. R. China

Supporting Information

ABSTRACT: The classical organic ferroelectric, poly(vinylidene fluoride) (PVDF), has attracted much attention as a promising candidate for data storage applications compatible with all-organic electronics. However, it is the low crystallinity, the large coercive field, and the limited thermal stability of remanent polarization that severely hinder large-scale integration. In light of that, we show a molecular ferroelectric thin film of [Hdabco][ReO₄] (dabco = 1,4-diazabicyclo[2.2.2]octane) (**1**), belonging to another class of typical organic ferroelectrics. Remarkably, it displays not only the highest Curie temperature of 499.6 K but also the fastest polarization switching of 100k Hz among all reported molecular ferroelectrics. Combined with the large remanent polarization values ($\sim 9 \mu\text{C}/\text{cm}^2$), the low coercive voltages ($\sim 10 \text{ V}$), and the unique multiaxial ferroelectric nature, **1** becomes a promising and viable alternative to PVDF for data storage applications in next-generation flexible devices, wearable devices, and bionics.



INTRODUCTION

Almost a century has passed since Rochelle salt (potassium sodium tartrate tetrahydrate) was discovered as the first ferroelectric with switchable spontaneous polarization under an external electric field.¹ From then on, the so-called ferroelectricity and the abundant related phenomena like dielectric, piezoelectric, pyroelectric, and electro-optic properties of ferroelectrics have been explored in numerous applications, including nonvolatile memory elements, capacitors, sensors, photovoltaics, and so on.¹ Despite years of efforts to develop new ferroelectric materials, currently inorganic ceramic ferroelectrics such as barium titanate (BTO) and lead zirconate titanate (PZT) are still the most studied and widely used ones with excellent performance characteristics.² Not insignificant, however, is the fact that these materials contain environmentally harmful heavy metals and usually require high-cost, high-temperature processing and high energy consumption. Against this background, organic ferroelectrics, which are lightweight, inexpensive, environmentally friendly, low acoustical impedance, biocompatible, and easy processing, become promising and viable alternatives to the conventional inorganic ones.³ The ferroelectric polymer poly(vinylidene fluoride) (PVDF) working at room temperature is just a representative one, which has been used for many piezoelectric and pyroelectric devices.⁴

Nevertheless, indeed PVDF suffers from low crystallinity, large coercive field, and narrow operational temperature range.⁵ Specifically, low crystallinity would induce the bad rectangularity of ferroelectric hysteresis loop, and large coercive field violates the demand of operating voltage lower than 10 V, both

of which are mainly responsible for the unrealized ferroelectric memory applications. Moreover, its polar properties would degrade above 353 K, seriously hampering the large-scale integration. Then, what on earth can researchers do to solve these issues? Maybe the answer can be found in another class of typical organic ferroelectrics, molecular ferroelectrics. So far, although much remarkable progress has been made in molecular ferroelectrics, they cannot share the most-valuable feature of PVDF, while the uniaxial characteristic makes them difficult to use in the film form.⁶ Taking, for example, croconic acid as an uniaxial ferroelectric, its bulk crystal sample has a remanent polarization ($P_r \sim 20 \mu\text{C}/\text{cm}^2$) comparable to that of BTO, whereas the P_r of the polycrystalline film is only $0.4 \mu\text{C}/\text{cm}^2$.^{3c,7} At this point, if they can possess a multiaxial nature that is preferable for gaining larger polarization after poling, molecular ferroelectrics might overcome the drawbacks and retain the advantages of PVDF.

Here, we present a multiaxial molecular ferroelectric thin film of [Hdabco][ReO₄] (dabco = 1,4-diazabicyclo[2.2.2]octane) (**1**), which exhibits two distinct transitions from paraelectric $m\bar{3}m$ to the ferroelectric $4mm$ (3 polar axes) at 499.6 K and to the ferroelectric m (12 polar axes) at 377.1 K, respectively. Using piezoresponse force microscopy (PFM), the polarization switching behaviors in the two ferroelectric phases are both clearly demonstrated. As far as we are aware, the Curie temperature of **1** (499.6 K) is the highest among the known molecular ferroelectrics, well above that of BTO (393 K).⁸

Received: July 23, 2017

Published: September 3, 2017

enabling a better thermal stability of the P_r than PVDF. More importantly, the thin film of **1** can display well-defined rectangular polarization–electric field (P – E) hysteresis loops even at a very high frequency of 100 kHz at room temperature, indicating the fastest polarization switching among the known molecular ferroelectrics, which is too difficult to achieve in PVDF.^{6a,c,9} In addition, it is the large P_r values ($\sim 9 \mu\text{C}/\text{cm}^2$) and the low coercive voltages ($V_c \sim 10 \text{ V}$) that afford it great potential for memory devices, compatible with low-power technology and all-organic electronics. With those benefits and excellent ferroelectric properties, **1** would be an ideal candidate for data storage applications in wearable devices, flexible materials, biomachines, and so on.

RESULTS AND DISCUSSION

At room temperature, the crystal of **1** was found to crystallize in the polar space group Cm (monoclinic point group m), with cell parameters of $a = 10.043(2)$, $b = 9.143(2)$, $c = 5.3525(10) \text{ \AA}$, $\beta = 90.86(3)^\circ$, and $V = 491.4(3) \text{ \AA}^3$, where the ferroelectric properties have been preliminarily revealed by the measurements of P – E hysteresis loops along [100] and [001].¹⁰ Meanwhile, Szafrański et al. also pointed out that **1** crystallizes in the centrosymmetric space group $P4/mmm$ above Curie temperature (T_c , 374 K), belonging to the paraelectric phase. However, after this report, our group measured the temperature dependence of the second harmonic generation (SHG) signal of compound **1** and found that the signal intensity above T_c is still nonzero.¹¹ Because Re^{7+} is a nonmagnetic cation, there should be no magnetic dipole contributing to the SHG effect. Consequently, the nonzero SHG intensity in **1** must be ascribed to its noncentrosymmetry structure, which is also verified by single crystal X-ray diffraction, that is, the space group is $P4mm$ and not $P4/mmm$. Then, is there a possibility that this polar phase is also a ferroelectric one? Unfortunately, until now no evidence has been presented about the ferroelectricity in this phase, as Szafrański et al. explained, “dielectric losses (ϵ'') along the $\text{NH}^+ \cdots \text{N}$ bonded chains parallel to the crystal direction [z] rise so drastically above 374 K that any polarization measurements along this direction are practically impossible”.¹⁰

Combining the results of SHG and differential scanning calorimeter (DSC) in ref 11, we can see that **1** undergoes three sequential phase transitions at 200.7 K (T_3), 377.1 K (T_2), and 499.6 K (T_1), respectively.¹¹ For convenience, we label the phase at above 499.6 K as phase I, the phase in temperature range of 377.1–499.6 K as phase II, the phase in temperature range of 200.7–377.1 K as phase III, and the phase at below 200.7 K as phase IV. Unfortunately, the single-crystal structure of phase I was not determined because of relatively weak intensity especially for those in the relatively high-angle region. Even so, the variable-temperature powder X-ray diffraction (PXRD) measurements were carried out to provide an insight into the crystal structure in the phase I. The PXRD pattern gained at 298 K matches well with the results simulated from the single-crystal structure at room temperature, unraveling the high crystallinity and purity of the phase, which is far better than that of PVDF (Figure S1). With the increase of temperature, the pattern at 423 K shows a little different, for example, some diffraction peaks at around 25° disappear, meaning the emergence of a new phase (Figure 1). Also, the fairly smaller number of peaks observed above T_1 at 508 K suggests that the symmetry of the Phase I becomes very high. The Pawley refinement of the PXRD diffraction data at 508 K

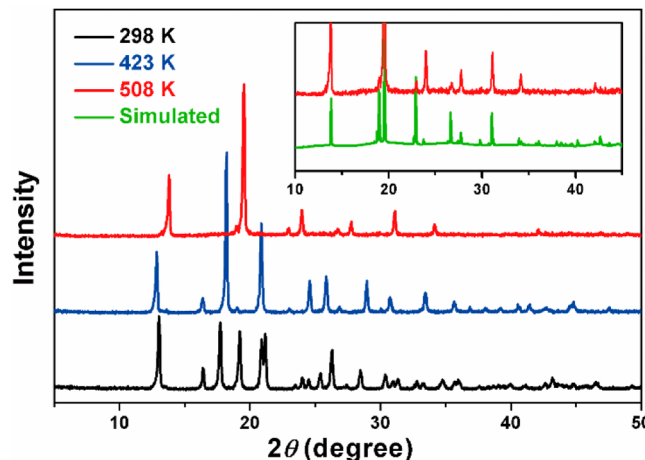


Figure 1. PXRD patterns of **1** measured in the temperature range of 298 to 508 K, showing two structural phase transitions. Insert: A comparison of the experimental PXRD pattern obtained at 508 K and the one simulated from the predicted paraelectric phase by Pawley refinements.

reveals a simple cubic unit cell with $a = 6.42427 \text{ \AA}$, and the suggested most possible space group is the centrosymmetric $Pn\bar{3}m$ (point group $m\bar{3}m$). The high symmetry indicates that the phase I is an isotropic plastic phase in which the molecules are nearly freely rotating and thus shows no polarization. This situation is very similar to that recently observed for the quinuclidinium salt which undergoes a ferroelectric transition.¹² The centrosymmetric structure corresponds to the paraelectric phase, in good agreement with the SHG result.

As shown in Figure S2, the crystal structures of phases II and III consist of ReO_4^- anions and monopronated dabco cations which form one-dimensional chains by hydrogen-bond interactions. The notable feature of these structures is that the monopronated dabco cations are oriented along the c axes. The packing of the anions and cations looks like that of the familiar simple cubic CsCl , that is, each cation is surrounded by eight anions, and vice versa. Phase II adopts the space group $P4mm$ (point group $4mm$), corresponding to the first ferroelectric phase. The cations and anions both exhibit orientational disorder due to the rotation along the axes parallel to the c axis (Figure 2a). For phase II, the symmetry change from the paraelectric phase to the ferroelectric phase is described by an Aizu notation of $m\bar{3}mF4mm$, like that observed in BTO, thus **1** should possess a multiaxial nature with three symmetry-equivalent polar axes in this phase, as shown in Figure 2c. Phase III adopts the space group Cm (point group m), corresponding to the second ferroelectric phase, where the lower symmetry results from the ordering of the cations and anions (Figure 2b). The symmetry change with an Aizu notation of $m\bar{3}mFm$ will allow the spontaneous polarization in the Phase III to be generated and switched along any of the 12 symmetry-equivalent ferroelectric axes (Figure 2d). The relationship of the cells of phase III and I is $b^{III} \approx a^I + b^I$, $a^{III} \approx -a^I + b^I$, $c^{III} \approx c^I$ (Figure 2b), while the cell of phase II can be derived by elongating the c axis of the phase II. Such a multiaxial characteristic is scarce among molecular ferroelectrics, which can offer a possibility for the polycrystalline sample (e.g., thin film) to obtain a larger polarization almost comparable to that of the single crystal. Accordingly, to promote practical applications, a systematic analysis and study

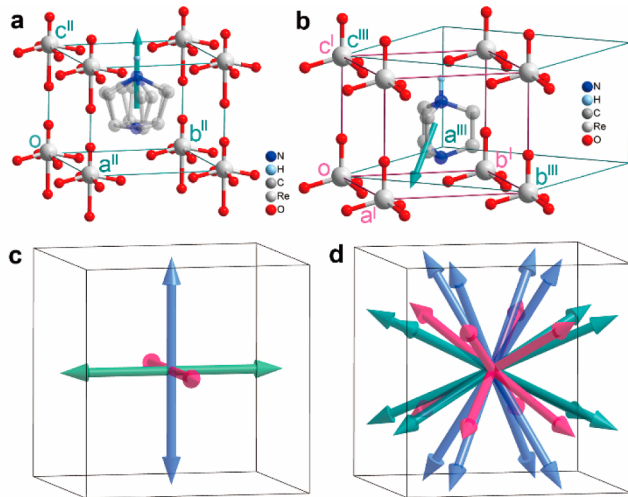


Figure 2. Perspective views of the crystal structure of (a) phase II and (b) phase III of **1**. The cell with pink edges represent the cell from that of the cubic phase I by lattice twist. (c, d) The scheme drawing of possible equivalent polarization directions in the phases II and III, respectively.

with respect to the ferroelectricity of the thin film was performed on **1**.

The spontaneous polarization with a hysteresis effect in the ferroelectric materials can be used as a memory function, and the high-density arrays of capacitors based on thin ferroelectric films are indeed used to make ferroelectric random access memories (FeRAMs) for computers and radio frequency identification (RFID) cards.¹³ The usage of thin films allows the high fields required to switch the polarization state to be achieved with a low voltage, making them suitable for integrated electronics applications. Hence, molecular ferroelectric like **1**, which can be easily fabricated as thin films by low-temperature and cost-saving solution methods, is a promising candidate for application in ferroelectric capacitors. The film preparation procedure of **1** is simply summarized below: A drop of the homogeneous precursor solution of [Hdabco][ReO₄] in deionized water was carefully deposited on a fresh cleaned indium tin oxide (ITO)-coated conductive glass, and then a high-coverage and continuous thin film comprising of needle-like crystals is grown on this substrate with controlled temperature (50 ± 1 °C). As illustrated in Figure S3, such a highly uniform shape and crystalline state in the large area is ideal for thin films used in devices. Using atomic force microscopy, the average film thickness of ~600 nm was revealed by a man-made gap on the film, which is the desired capacitor thickness (Figure S4).

For the sake of testing the ferroelectricity of the as-grown thin film of **1**, a drop of liquid GaIn eutectic was placed on this high-quality thin film and acted as the top electrode, while the ITO-coated glass was taken as the bottom electrode to form a capacitor with GaIn/thin-film/ITO architecture. Based on this capacitor geometry, at room temperature, with the AC frequency increasing from 1k to 100k Hz, the *P-E* hysteresis loops of the thin film always retain good rectangularity (Figure 3). The ferroelectric polarization could be switchable at the really high frequency of 100k Hz, which is the highest frequency limit of our measurements, where the ferroelectric loop still completely opens to reach saturation, meaning a great possibility for the faster polarization switching of **1**. Such a high

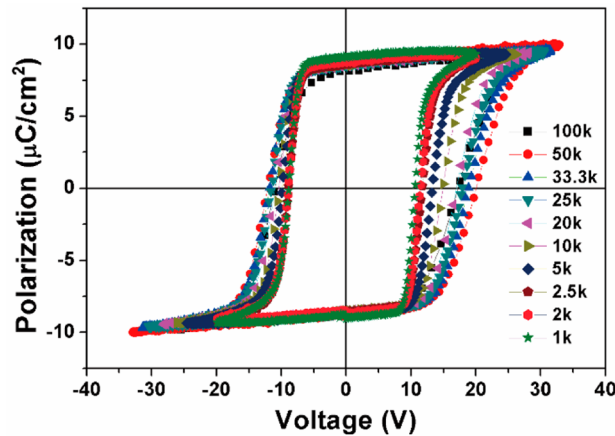


Figure 3. Room-temperature ferroelectric hysteresis loops of the thin film of **1** at different AC frequencies (Hz).

frequency, even higher by an order of magnitude than that reported in the thin film of [Hdabco]ClO₄, would open a new avenue toward the application in ferroelectric memories.^{6a} The P_r and V_c were determined from the intercepts in the *P-E* hysteresis loops with different AC frequencies. The reasonably large P_r values, about 9 $\mu\text{C}/\text{cm}^2$ at room temperature, close to those of the theoretical values,^{10,11} are significantly greater than those in the recently reported multiaxial molecular ferroelectric thin films and comparable to that of PVDF.^{3b} The V_c values, which range from 10 to 20 V, depending on the frequency, can meet the demand that an operating voltage should be lower than 10 V, compatible with low-power technology and all-organic electronics. Unfortunately, however, the ferroelectricity still can not be observed in the phase II using the *P-E* hysteresis loop measurements. This might be because the increasing leakage currents, accompanied by the large dielectric losses, make the breakdown field close to the coercive field at phase II in the thin film of **1**, thus the polarization switching is difficult to realize.

In ferroelectric materials, the piezoelectric effect is a direct proof of the existence of polarization, hence PFM is an effective characterization tool for the study of polarization distribution within domains at the nanometer scale.¹⁴ For the thin film of **1**, PFM has been performed to study the ferroelectric domain structure and domain dynamics in both two ferroelectric phases. The PFM piezoresponse detected by the tip includes amplitude and phase signals that represent the magnitude of the local piezoelectric response and the polarization direction in each individual domain, respectively. The single-domain structure was mainly found in the as-grown thin film of **1**, on account of the uniform vertical PFM (VPFM) phase signal (Figure 4a). Then we carried out local polarization manipulation experiments to directly visualize the domain switching process, where the above-mentioned single-domain pattern was used as initial state. When a DC tip bias of -30 V was used to scanning the central zone, the resultant VPFM phase image is described by two-color tones with a contrast of 180°, which correspond to the two opposite polarization directions and indicate 180° polarization switching of the domain (Figure 4b). Moreover, the polarization in the emerging domain can be switched back and forth by applying a ±30 V voltage of opposite polarity (Figure 4c,d). Meanwhile, during the above domain manipulation, the surface morphology of the thin film remains constant, meaning that poling does not

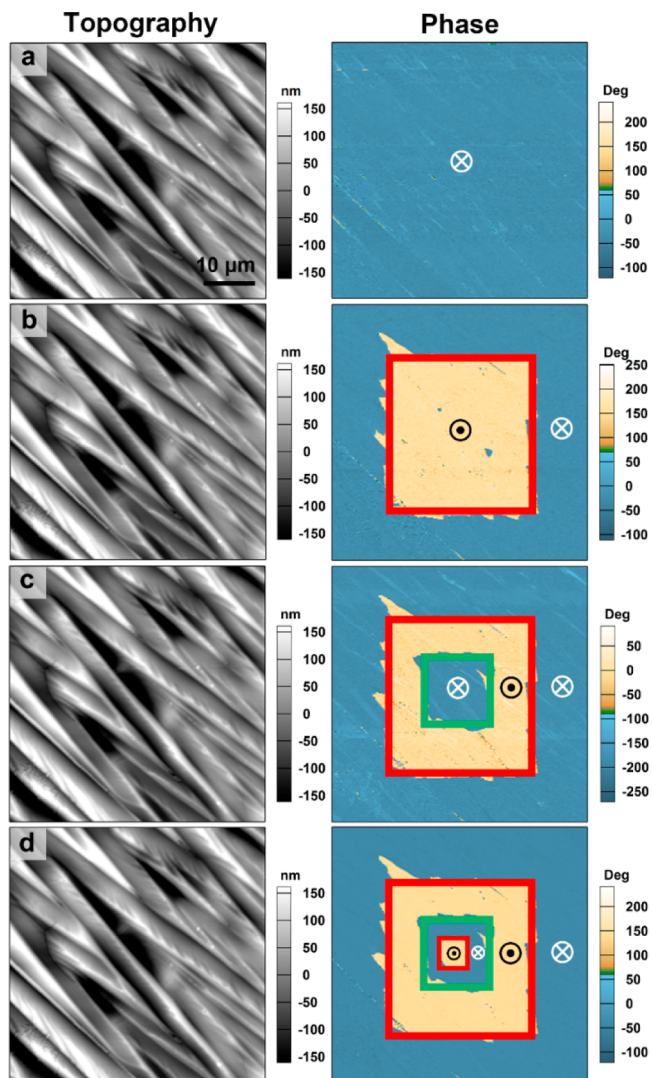


Figure 4. VPFM images of **1** in the phase III indicating ferroelectric polarization switching. Topography (left) and phase (right) images for the $50 \times 50 \mu\text{m}^2$ area of the thin film of **1**, which were taken (a) in the as-grown state and taken after applying tip biases of (b) -30 V , (c) subsequently $+30 \text{ V}$, and (d) finally -30 V in the central region. \ominus and \oplus correspond to their antiparallel directions of ferroelectric polarizations oriented upward and downward, respectively.

influence the surface topography. Such switchable polarization, the characteristic feature of a ferroelectric material, suggests the ferroelectricity in the phase III.

Next, we also provide solid evidence of the presence of polarization in the phase II. As given in Figure S5, a box-in-box domain pattern of the thin film of **1** was triggered by the forth-to-back switching of polarization at room temperature. With a rise of temperature up to 343 K, the written domains are still stable and remain unchanged (Figure S6a). Additionally, further increase of the temperature to 403 K does not lead to the vanishing of the domain structure, where only the slight movement appears for the domain walls, as shown in the phase and amplitude images (Figure S6b). This observation fully demonstrates that the spontaneous polarization still exists in the phase II, consistent well with the results of SHG and X-ray diffraction. With a drop in temperature, Figure S6c depicts the evolution of the ferroelectric domain structures achieved at room temperature. Note that the domain pattern in the

annealed state is strikingly different from the as-grown ferroelectric domain structure, due to the regrowth of ferroelectric domains induced by the symmetry breaking during the ferroelectric-to-ferroelectric phase transition.

In the annealed state of phase III, we can observe the abundant domains with different spontaneous polarization directions. For a more unambiguous visualization of the domain structures, the vertical and lateral PFM (VPFM and LPFM) images have been simultaneously acquired and analyzed in a smaller area of $12 \mu\text{m} \times 12 \mu\text{m}$ (marked with a red box in the phase image of Figure S6c). It is notable that the domain distribution in the vertical mode is similar to, but not identical to that in the lateral mode, signifying the presence of multiple polarization directions. Also, ferroelectric domains are not correlated with topographic surface features. As presented in the pink boxes of Figure 5, two phase images show the same

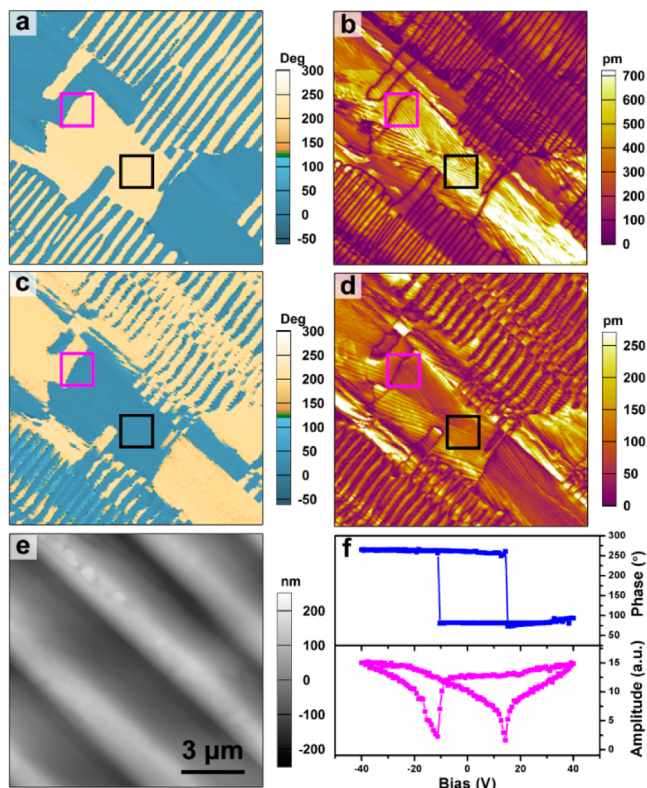


Figure 5. VPFM phase (a, c) and amplitude images (b, d) and topographic image (e) for the thin film of **1** at phase III. (f) VPFM phase and amplitude signals as functions of the tip voltage for a selected point at phase III, showing local PFM hysteresis loops.

bipolar domain pattern. Meanwhile, on both sides of the domain wall whose signal is necessarily null in the amplitude images, the piezoresponses in the two domains are uniform, which reveals the existence of 180° domain wall. In the region marked with black boxes, the homogeneous signals in the two phase images indicate the same directions in these two components, while obvious small stripe patterns with different contrasts appear in the amplitude images, suggesting the presence of non- 180° domain walls. Most importantly, a great many of stripe domains with various orientations are full of the entire area. This observation clearly uncovers the coexistence of multiple polarization orientations in the phase III of **1**.

PFM hysteresis loops shown in Figure 5f further demonstrate the ferroelectric nature of the phase III, wherein the local

coercive voltage is about 12.8 V. Similarly, the phase II can also exhibit bipolar piezoelectric hysteresis loops, and its local coercive voltage is about 17.2 V, larger than that in the phase III, allowing the polarization more difficult to be switched (Figure S7). Very importantly, we can intuitively observe the polarization switching process in the phase II by performing local domain manipulation experiments using PFM at 403 K. In the initial state, the VPFM phase signal is identical in the selected area of $30 \mu\text{m} \times 30 \mu\text{m}$, in accordance with the single-domain pattern (Figure 6a). After the center zone of this area

ferroelectricity. Therefore, the Curie temperature is T_1 at 499.6 K, which is the highest among the known molecular ferroelectrics. In addition, a perfect ferroelectric hysteresis loop can be achieved in the thin film at a frequency as high as 100 kHz at room temperature, with the large P_r values ($\sim 9 \mu\text{C}/\text{cm}^2$) and the low V_c ($\sim 10 \text{ V}$), very favorable to promote application in the ferroelectric memories. Combined with solution processability, lightweight, flexibility, and nontoxicity, **1** would be an ideal candidate for data storage applications in wearable devices, flexible materials, biomachines, and so on.

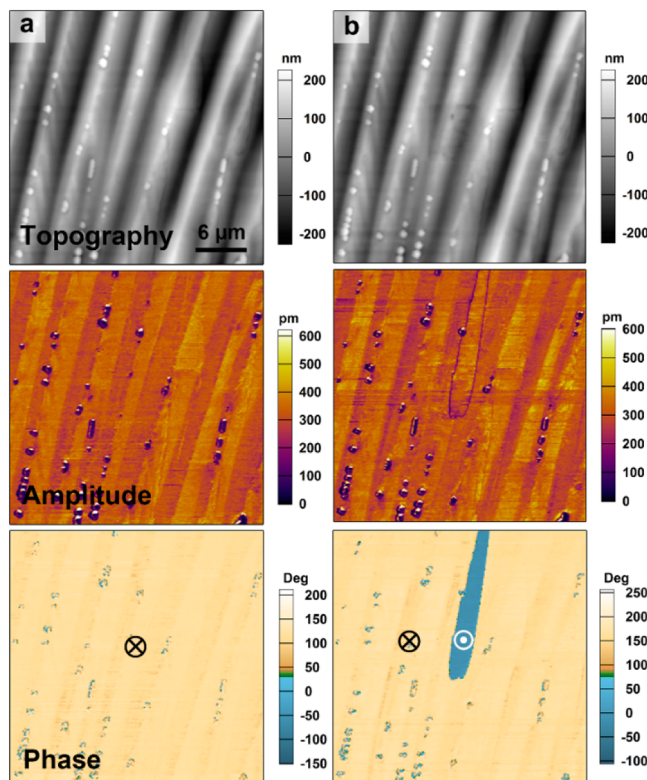


Figure 6. Panels in each column are arranged as the sequence: topographic images (top), then VPFM amplitude (middle), and last phase (bottom) images of the film surface in the phase II. (a) Initial state. (b) After the first switching produced by scanning with the tip bias of -35 V .

was rescanned with a DC tip-bias of -35 V , a clear bipolar domain pattern emerges in the phase image, and the corresponding domain wall is apparent in the amplitude image, manifesting the polarization switching of ferroelectric domain (Figure 6b). All the above evidence unambiguously establish the existence of ferroelectricity in the phase II, so the Curie temperature of **1** should be T_1 and not T_2 . Such a record-high Curie temperature (Table S1 and S2) makes it outstanding because of the adaptability to applications ranging from room temperature to unusual high temperature.

CONCLUSION

In summary, we present a multiaxial molecular ferroelectric thin film of $[\text{Hdabco}][\text{ReO}_4]$ (**1**), prepared by a simple and effective solution deposition method. It undergoes three sequential phase transitions at 499.6, 377.1, and 200.7 K, separated by four phases $\bar{m}\bar{3}m$, $4mm$, m , and $mm2$, respectively. Using PFM, we directly observed the polarization switching of ferroelectric domains in the ferroelectric phases II and III, confirming their

EXPERIMENTAL SECTION

Materials. All reagents and solvents in the syntheses were of reagent grade and used without further purification. **1** was prepared by slow evaporation of the ethanol solution of dabco and HReO_4 in a 1:1 molar ratio. The powder of **1** was dissolved in purified water to form a solution with a solubility of about 20 mg/mL. With this solution, thin films were deposited on ITO-coated glass substrates.

Measurements. $P-E$ hysteresis loops measurements are described elsewhere.^{6c} Nanoscale polarization imaging and local switching spectroscopy were carried out using a resonant-enhanced piezoresponsive force microscopy (MFP-3D, Asylum Research). Conductive Pt/Ir-coated silicon probes (EFM, Nanoworld) were used for domain imaging and polarization switching studies.

ASSOCIATED CONTENT

S Supporting Information

The Supporting Information is available free of charge on the ACS Publications website at DOI: 10.1021/jacs.7b07715.

Figures S1–S7, Tables S1–S2 and discussion (PDF)

AUTHOR INFORMATION

Corresponding Authors

*youyumeng@seu.edu.cn

*xiongrg@seu.edu.cn

ORCID

Ren-Gen Xiong: 0000-0003-2364-0193

Notes

The authors declare no competing financial interest.

ACKNOWLEDGMENTS

This work was supported by 973 project (2014CB932103) and the National Natural Science Foundation of China (21290172, 91422301, and 21427801).

REFERENCES

- (1) Lines, M. E.; Glass, A. M. *Principles and applications of ferroelectrics and related materials*; Clarendon Press: Oxford, UK, 1977.
- (2) (a) Scott, J. F. *Science* **2007**, *315*, 954. (b) Scott, J. F.; Araujo, C. P. d. *Science* **1989**, *246*, 1400.
- (3) (a) Horiuchi, S.; Tokura, Y. *Nat. Mater.* **2008**, *7*, 357. (b) Fu, D. W.; Cai, H. L.; Liu, Y.; Ye, Q.; Zhang, W.; Zhang, Y.; Chen, X. Y.; Giovannetti, G.; Capone, M.; Li, J.; Xiong, R. G. *Science* **2013**, *339*, 425. (c) Horiuchi, S.; Tokunaga, Y.; Giovannetti, G.; Picozzi, S.; Itoh, H.; Shimano, R.; Kumai, R.; Tokura, Y. *Nature* **2010**, *463*, 789. (d) Tayi, A. S.; Shveyd, A. K.; Sue, A. C.; Szarko, J. M.; Rolczynski, B. S.; Cao, D.; Kennedy, T. J.; Sarjeant, A. A.; Stern, C. L.; Paxton, W. F.; Wu, W.; Dey, S. K.; Fahrenbach, A. C.; Guest, J. R.; Mohseni, H.; Chen, L. X.; Wang, K. L.; Stoddart, J. F.; Stupp, S. I. *Nature* **2012**, *488*, 485. (e) Sato, O. *Nat. Chem.* **2016**, *8*, 644. (f) Li, W.; Wang, Z.; Deschler, F.; Gao, S.; Friend, R. H.; Cheetham, A. K. *Nat. Rev. Mater.* **2017**, *2*, 16099. (g) Tayi, A. S.; Kaeser, A.; Matsumoto, M.; Aida, T.; Stupp, S. I. *Nat. Chem.* **2015**, *7*, 281.

- (4) (a) Bune, A. V.; Fridkin, V. M.; Ducharme, S.; Blinov, L. M.; Palto, S. P.; Sorokin, A. V.; Yudin, S. G.; Zlatkin, A. *Nature* **1998**, 391, 874. (b) Naber, R. C.; Asadi, K.; Blom, P. W.; de Leeuw, D. M.; de Boer, B. *Adv. Mater.* **2010**, 22, 933. (c) Lang, S. B.; Muensit, S. *Appl. Phys. A: Mater. Sci. Process.* **2006**, 85, 125. (d) Ueberschlag, P. *Sens. Rev.* **2001**, 21, 118.
- (5) (a) Li, M.; Wondergem, H. J.; Spijkman, M. J.; Asadi, K.; Katsouras, I.; Blom, P. W.; de Leeuw, D. M. *Nat. Mater.* **2013**, 12, 433. (b) Whatmore, R. *Rep. Prog. Phys.* **1986**, 49, 1335. (c) Hu, Z.; Tian, M.; Nysten, B.; Jonas, A. M. *Nat. Mater.* **2009**, 8, 62.
- (6) (a) Tang, Y.-Y.; Zhang, W.-Y.; Li, P.-F.; Ye, H.-Y.; You, Y.-M.; Xiong, R.-G. *J. Am. Chem. Soc.* **2016**, 138, 15784. (b) Ye, H.-Y.; Ge, J.-Z.; Tang, Y.-Y.; Li, P.-F.; Zhang, Y.; You, Y.-M.; Xiong, R.-G. *J. Am. Chem. Soc.* **2016**, 138, 13175. (c) Shi, P.-P.; Tang, Y.-Y.; Li, P.-F.; Ye, H.-Y.; Xiong, R.-G. *J. Am. Chem. Soc.* **2017**, 139, 1319. (d) Pan, Q.; Liu, Z. B.; Tang, Y. Y.; Li, P. F.; Ma, R. W.; Wei, R. Y.; Zhang, Y.; You, Y. M.; Ye, H. Y.; Xiong, R. G. *J. Am. Chem. Soc.* **2017**, 139, 3954. (e) Xu, W.-J.; Li, P.-F.; Tang, Y.-Y.; Zhang, W.-X.; Xiong, R.-G.; Chen, X.-M. *J. Am. Chem. Soc.* **2017**, 139, 6369. (f) Li, P. F.; Tang, Y. Y.; Wang, Z. X.; Ye, H. Y.; You, Y. M.; Xiong, R. G. *Nat. Commun.* **2016**, 7, 13635. (g) You, Y. M.; Tang, Y. Y.; Li, P. F.; Zhang, H. Y.; Zhang, W. Y.; Zhang, Y.; Ye, H. Y.; Nakamura, T.; Xiong, R. G. *Nat. Commun.* **2017**, 8, 14934.
- (7) Jiang, X.; Lu, H.; Yin, Y.; Zhang, X.; Wang, X.; Yu, L.; Ahmadi, Z.; Costa, P. S.; DiChiara, A. D.; Cheng, X.; Gruverman, A.; Enders, A.; Xu, X. *Appl. Phys. Lett.* **2016**, 109, 102902.
- (8) Haertling, G. H. *J. Am. Ceram. Soc.* **1999**, 82, 797.
- (9) Cai, H.-L.; Zhang, W.; Ge, J.-Z.; Zhang, Y.; Awaga, K.; Nakamura, T.; Xiong, R.-G. *Phys. Rev. Lett.* **2011**, 107, 147601.
- (10) Szafrański, M.; Katrusiak, A.; McIntyre, G. *Phys. Rev. Lett.* **2002**, 89, 215507.
- (11) Cai, H.-L.; Fu, D.-W.; Zhang, Y.; Zhang, W.; Xiong, R.-G. *Phys. Rev. Lett.* **2012**, 109, 169601.
- (12) Harada, J.; Shimojo, T.; Oyamaguchi, H.; Hasegawa, H.; Takahashi, Y.; Satomi, K.; Suzuki, Y.; Kawamata, J.; Inabe, T. *Nat. Chem.* **2016**, 8, 946.
- (13) Scott, J. F. *Ferroelectric memories*; Springer Science & Business Media: Washington, D.C., 2013; Vol. 3.
- (14) (a) Balke, N.; Winchester, B.; Ren, W.; Chu, Y. H.; Morozovska, A. N.; Eliseev, E. A.; Huijben, M.; Vasudevan, R. K.; Maksymovych, P.; Britson, J.; Jesse, S.; Kornev, I.; Ramesh, R.; Bellaiche, L.; Chen, L. Q.; Kalinin, S. V. *Nat. Phys.* **2011**, 8, 81. (b) Kalinin, S. V.; Rodriguez, B. J.; Jesse, S.; Karapetian, E.; Mirman, B.; Eliseev, E. A.; Morozovska, A. N. *Annu. Rev. Mater. Res.* **2007**, 37, 189. (c) Lee, D.; Lu, H.; Gu, Y.; Choi, S.-Y.; Li, S.-D.; Ryu, S.; Paudel, T. R.; Song, K.; Mikheev, E.; Lee, S.; Stemmer, S.; Tenne, D. A.; Oh, S. H.; Tsymbal, E. Y.; Wu, X.; Chen, L.-Q.; Gruverman, A.; Eom, C. B. *Science* **2015**, 349, 1314. (d) Lu, H.; Bark, C. W.; Esque de los Ojos, D.; Alcala, J.; Eom, C. B.; Catalan, G.; Gruverman, A. *Science* **2012**, 336, 59. (e) Garcia, V.; Fusil, S.; Bouzehouane, K.; Enouz-Vedrenne, S.; Mathur, N. D.; Barthelemy, A.; Bibes, M. *Nature* **2009**, 460, 81.